The calm and variable inner life of the Atlantic Intertropical Convergence Zone: the relationship between the doldrums and surface convergence

J. M. Windmiller [1]

[1]Max Planck Institute for Meteorology, Hamburg, Germany

Key Points:

- The doldrums are confined to the area of time-mean convergence of the Atlantic ITCZ.
- The frequency distribution of low wind speed events peaks between the edges of the ITCZ, which are characterized by increased convergence.
- Low wind speed events within the ITCZ occur when precipitation is absent, suggesting they coincide with local low-level divergence.

Corresponding author: Julia Windmiller, julia.windmiller@mpimet.mpg.de

Abstract

The doldrums are regions of low wind speeds and variable wind directions in the deep tropics that have been known for centuries. Although the doldrums are often associated with the Intertropical Convergence Zone (ITCZ), the exact relationship remains unclear. This study re-examines the relationship between low-level convergence and the Atlantic doldrums. By analyzing the frequency distribution of low wind speed events in reanalysis and buoy data, we show that the doldrums are largely confined between the edges of the ITCZ marked by enhanced surface convergence. While the region between the edges is a region of high time-mean precipitation, low wind speed events occur in the absence of precipitation. We therefore hypothesize that low wind speed events occur in regions of low level divergence rather than convergence.

Plain Language Summary

The doldrums, an area between the trade winds formerly feared by mariners because of its low wind speeds and variable wind directions, have largely disappeared from mention in the scientific literature. The most commonly given explanation for the existence of the doldrums, according to which the weaker surface winds result from the upward circulation of the trade winds, can only be true when averaged over timescales of days or weeks. In this study, we re-examine this region and its relationship to the convergence of the trade winds. We show that although low wind speed events occur in the region where the trade winds meet and precipitation rates are high on average, they occur precisely when there is no precipitation. This leads us to the hypothesis that these regions of low wind speeds are characterised by sinking rather than rising air.

1 Introduction

"Day after day, / day after day, / We stuck, nor breath nor motion; / As idle as a painted ship / Upon a painted ocean" is how S. T. Coleridge described the doldrums in the 1834 poem *The Rime of the Ancient Mariner*. Located between the trades, the doldrums were feared for their low wind speeds and variable wind directions by mariners when sailing ships were still the primary means of sea transportation (e.g., Maury, 1855). While still relevant to circumnavigators today (e.g., Herrmann & Wolfers, 2021), their decreasing economic importance went hand in hand with decreasing scientific interest and, until recently, mention of the doldrums had largely disappeared from the scientific literature (Klocke et al., 2017).

Due to their location between the trade winds, the doldrums have long been associated with the convergence of the trade winds in what is now known as the Intertropical Convergence Zone, ITCZ (Durst, 1926; Fletcher, 1945; Gordon, 1951; Gentilli, 2005). As the terms doldrums and ITCZ were used almost synonymously in the early literature, it is difficult to separate discussions of the ITCZ in general from discussions of the doldrums, especially their characteristic low wind events. For example, Durst (1926) describes the doldrums as a region within the equatorial trough with vanishing meridional pressure gradients, large-scale low-level convergence, and vertical ascent. He also notes that this region is characterized by strong and frequent precipitation. According to this description, low meridional wind speeds result from low-level convergence of the trade winds and low (geostrophic) zonal wind speeds result from the absence of a meridional pressure gradient. However, this description can only explain low wind speeds in the mean, i.e. when averaged over time scales of days or weeks. At any given time, the ITCZ is characterised by rapid ascent through convective clouds but descent through the environment, which comprises the majority of the area even in regions of active convection (Riehl & Malkus, 1958; Yanai et al., 1973). As in the case of the convective updrafts, low-level

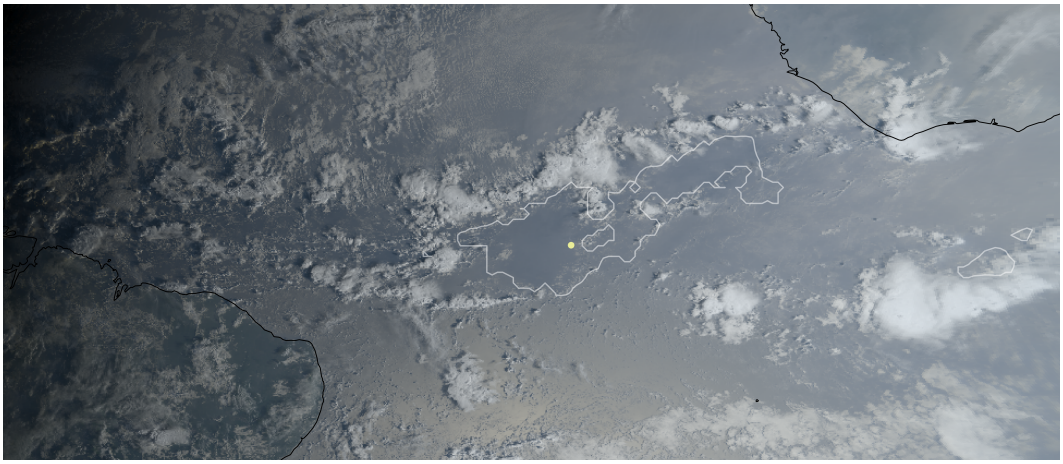

Figure 1. Natural color image of the Atlantic ITCZ from NOAA Geostationary Operational Environmental Satellites (GOES) 16 satellite on 4 February, 2023 at 09:30 UTC. The solid white line indicates the $3\,\mathrm{m\,s^{-1}}$ contour of the 10 meter wind speed as measured by the Special Sensor Microwave Imager Sounder (4 February, 2023; descending). The yellow dot denotes the position of RV Maria S. Merian.

convergence is usually highly localized, e.g., in the form of convergence lines (Weller et al., 2017).

Recently Windmiller and Stevens (2024) showed that the Atlantic ITCZ has an inner life, i.e., a rich dynamic and thermodynamic structure with substantial day-to-day variation. They found that the ITCZ is characterized by reduced meridional wind speeds between two edges of enhanced convergence. This raises the question of whether the doldrums mark the inner part of the ITCZ. This, at least, is what we observed during a recent campaign aboard the German RV Maria S. Merian in the boreal winter of 2023. During the campaign, three north-south transects of the East Atlantic ITCZ were completed and, as described in detail in Köhler et al. (2024), we observed regions of very low wind speeds between the edges of the ITCZ, as determined from the meridional wind speed component (Windmiller & Stevens, 2024). The wind speeds were particularly low during our last crossing, where the southern edge of the region of low wind speeds also marked the southern edge of the ITCZ, see Fig. 1, with hourly mean wind speeds of about $1\,\mathrm{m\,s^{-1}}$ at the time of the satellite image. The reduced wind speeds are actually visible as relatively dark regions on the natural color satellite image, because the low wind speeds lead to low wave heights (and sufficient distance from the point of specular reflection) leads to less scattering in the direction of the satellite (Cox & Munk, 1954).

In this study, we re-examine the doldrums and their day-to-day variation, focusing on their characteristic low wind speed events and how these relate to low-level convergence. To this end, we analyze low wind speed events in reanalysis and buoy data. The data sets used are described in detail in section 2. The methods used to identify the doldrums, the edges of the ITCZ, and a compositing method to investigate the temporal evolution of low wind speed events are presented in section 3. The frequency distribution of low wind speed events as a function of season, latitude, longitude, and distance from the ITCZ edge is presented in Section 4, where we also analyze the relationship with precipitation. In section 5, we summarize our results and propose the hypothesis that the low wind speed events in the doldrums are caused by surface divergence and subsiding motion rather than surface convergence and ascending motion.

2 Data

To investigate the relationship between the ITCZ and the doldrums we use data from the Pilot Research Moored Array in the tropical Atlantic (PIRATA, Bourlès et al., 2008) as well as the 5th Generation of the ECMWF (European Centre for Medium-Range Weather Forecasts) Reanalysis of meteorological data (ERA5, Hersbach et al., 2018). To investigate the latitudinal and longitudinal dependence, we use three of the PIRATA buoys in the western Atlantic along 38°W (4°N, 8°N, 12°N) and three of the PIRATA buoys in the eastern Atlantic along 23°W (0°, 4°N, 12°N). The variables considered are air temperature (measured at a height of 3 m), precipitation (measured at a height of 3.5 m), and wind speed (measured at a height of 4 m). We use data with the highest temporal resolution available, which corresponds to 10-minute data for all variables considered. All measurements where the quality code indicated either "Lower Quality" (quality code 4) or "Sensor or Tube Failed" (quality code 5) were removed. All other data available at the time of analysis were used. The earliest data analyzed is from 01/30/1998 and the latest data is from 03/08/2018. For each buoy we have between 7.5 years (12°N 23°W) and 14.1 years (8°N 38°W) of data. To complement the buoy data, we use twenty years of hourly ERA5 data (horizontal resolution of 0.25° x 0.25°), from August 18, 2001 to August 17, 2021, centered at 38°W and 23°W and extending from 10°S to 20°N. To focus on the doldrums over the ocean, a land-sea mask was applied to mask all land grid cells. The variables we use are the hourly averaged precipitation rate, the vertically integrated total column water vapor, and the two 10 meter horizontal wind components $\vec{v}_{10m}$. From the horizontal wind components we calculate the wind speed, $|\vec{v}_{10m}|$, and the divergence field, $\nabla \cdot \vec{v}_{10m}$, using metpy (version 1.4.1, May et al., 2016). For each of these fields, three-degree zonal averages are computed, centered on the longitudes of the buoys, i.e. 39.5°W to 36.5°W and 24.5°W to 21.5°W.

3 Method

In the following we investigate the relationship between the low wind speed events that characterize the doldrums and the surface convergence in the ITCZ. Low wind speed events are defined as extended and/or persistent regions of wind speeds less than $3\,\mathrm{m\,s^{-1}}$. This threshold, previously used by Klocke et al. (2017), is also roughly equivalent to 5 knots, often stated as the minimum wind speed for sailing. For the buoy data, we require the wind speed to be below the threshold wind speed for at least six hours to classify as a low wind speed event. For the reanalysis data, we define a low wind speed event to occur at a given time and latitude whenever the three-degree zonally averaged wind speed is below the threshold wind speed. To calculate the mean occurrence rate of low wind speed events from the reanalysis data, we introduce a new binary field which indicates the presence (1) or absence (0) of a low wind speed event. Next, we introduce three methods to investigate the relationship between low wind speed events and surface divergence on *multi-day timescales*, *hourly timescales*, and by considering the *temporal evolution* of the low wind speed events.

Multi-day timescales

As discussed in the introduction, on time scales of days or weeks, we expect the low wind events to occur in the region of mean convergence that characterizes the ITCZ. To test this, we first compute five-day averages (excluding the last day of the year if it is a leap year) for the low wind speed event field and the divergence field of the reanalysis data. For each five-day interval, we then calculate the average over all years. In the thus averaged 10-meter divergence field the region of mean convergence is defined as the region where the divergence is less than zero. As surface convergence is not the only way to identify the location of the ITCZ, we also use the column water vapour field and the precipitation field. Following Masunaga (2023), we use the 50 mm threshold in column

water vapour to identify the edge of the ITCZ by the presence of a sharp gradient in moisture (Mapes et al., 2018; Masunaga & Mapes, 2020) and, following Wodzicki and Rapp (2016), we use a $2.5\,\mathrm{mm\,d^{-1}}$ threshold in precipitation. Finally, we also consider the five-day mean latitude of the northern and southern edges of the ITCZ calculated from the hourly values of surface convergence, as described in detail below.

Hourly timescales

We next test the hypothesis that on short time scales low wind speed events occur predominantly between the edges of the ITCZ. We identify the edges of the ITCZ based on the hourly ERA5 surface convergence field ($-\nabla\cdot\vec{v}_{10m}$) using a slightly modified version of the peak convergence strength method presented in Windmiller and Stevens (2024). For each instance in time we identify the latitudes of peak convergence, using the SciPy "find_peaks" function (version 1.8.1; Virtanen et al., 2020). To identify a local maximum in convergence as a peak, we set the required prominence and the height of the peaks to be equal to the 90th percentile of the convergence field calculated for all times and latitudes at the respective longitude. We then identify the northern and southern edges of the ITCZ as the latitude of the northernmost and southernmost convergence peak, respectively. To ensure that the outermost convergence lines related to the ITCZ are identified, this last step differs from the method described in Windmiller and Stevens (2024), where the edges were set equal to the two strongest convergence peaks. In cases where at least two convergence peaks are identified, we assess the relationship between the low wind speed events and the ITCZ edges thus identified, by rescaling the latitudes of the low wind speed event field as well as the convergence field by

$$\phi_{\mathrm{scale}} = (\phi - \phi_{\mathrm{south}})\frac{\langle\phi_{\mathrm{north}} - \phi_{\mathrm{south}}\rangle}{\phi_{\mathrm{north}} - \phi_{\mathrm{south}}} + \langle\phi_{\mathrm{south}}\rangle, \tag{1}$$

where ϕ_{south} is the southernmost and ϕ_{north} is the northernmost of the detected convergence peaks and $\langle\cdot\rangle$ denotes a temporal average over the whole dataset. The rationale for this scaling is to remove the smoothing of the dynamic and thermodynamic structure of the ITCZ that results from shifts in the latitudinal position and width of the ITCZ on seasonal but also sub-seasonal timescales.

Temporal evolution

Finally, we consider the relationship between convergence and the temporal evolution of low wind speed events using the buoy data. As we cannot calculate convergence from single point measurements, we use precipitation as a proxy for storm scale divergence and convergence. For individual storms, we expect low-level convergence to be associated with updraft formation and thus to precede precipitation formation, and low-level divergence to be associated with downdraft formation and thus to follow or coincide with precipitation formation (e.g., Byers & Braham, 1949). We address the question of whether the low wind speed events occur before or after the onset of precipitation by computing composites with respect to the onset time of the low wind speed events (t_{onset}), where the onset time of the low wind speed event is defined as the first time the wind speed drops below the threshold wind speed. To assess whether the precipitation rates before or during the low wind speed events are in general above or below average, we determine the month with the most frequent low wind speed events for each buoy and calculate the corresponding multiyear average precipitation rate for that month. This last step is necessary because the average precipitation rate observed at the buoys varies significantly throughout the year due to the seasonal cycle of the ITCZ. In general, this re-scaling is not limited to the wind speed or precipitation field, but can be applied to any other field. We will use this to investigate the temporal evolution of the surface air temperature, where convective downdrafts manifest themselves in the form of temperature drops.

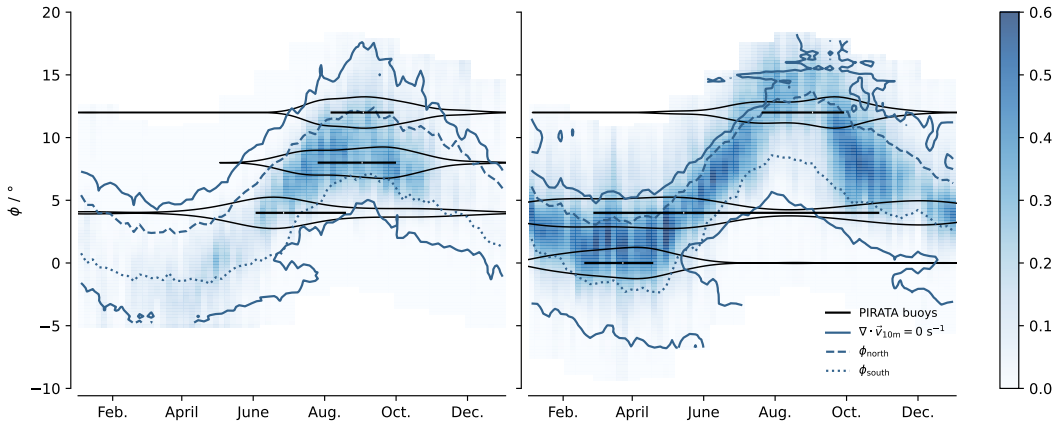

Figure 2. Seasonal cycle of the frequency of low wind speed events (left) around 38°W and (right) 23°W as calculated from reanalysis data (blue shading) and buoy data (black violins). The edges of the ITCZ are shown as calculated from (solid blue line) zero divergence and (dashed blue line) the northern and (dotted blue line) southern convergence peaks.

4 Results

Multi-day timescales

Figure 2 shows that the latitudinal extent of the East and West Atlantic doldrums has a seasonal cycle that follows the seasonal cycle of the ITCZ. This is shown by both the reanalysis and the buoy data. While the region of mean low-level convergence defines a broad latitudinal band containing almost all low wind speed events, the northern and southern edges of the ITCZ, calculated from ϕ_{south} and ϕ_{north}, match the edges of the doldrums much more closely. We find a similar agreement between the latitudinal extent of the ITCZ when determined by CWV or precipitation (not shown). In addition to the latitudinal dependence, the frequency of occurrence of low wind speed events is also strongly dependent on the season and the region. Low wind speed events are generally more frequent in the eastern than in the western Atlantic. The frequency of low wind speed events in the west peaks during boreal summer, when the ITCZ is at it's northernmost position, while in the east it peaks during boreal spring, when the ITCZ is at it's southernmost position. Thus, while the ITCZ edges bound the region in which low wind speed events occur throughout the year, the actual frequency of low wind events within the ITCZ depends on season and region.

Hourly timescales

How does this picture change if we identify the ITCZ on hourly rather than multi-day time scales? Figure 3 shows the low wind speed frequency together with the divergence and the precipitation field in the rescaled coordinates introduced in Eq. 1. As noted above, the prominence in the convergence field to qualify as a convergence peak has to be larger than the 90th percentile which leads to at least two peaks detected in 70.2% of the cases in the western Atlantic and 72.6% of the cases in the eastern Atlantic. The divergence field in Fig. 3 shows two pronounced convergence peaks, as expected from the design of the method. These convergence peaks correspond to the northern and southern edges of the latitudinal band with the highest frequency of low wind speed events as well as precipitation. While the distribution of low wind speed events in the western Atlantic is mostly symmetric with respect to the northern and southern convergence line, there is a marked asymmetry in the occurrence of low wind speed events in the eastern

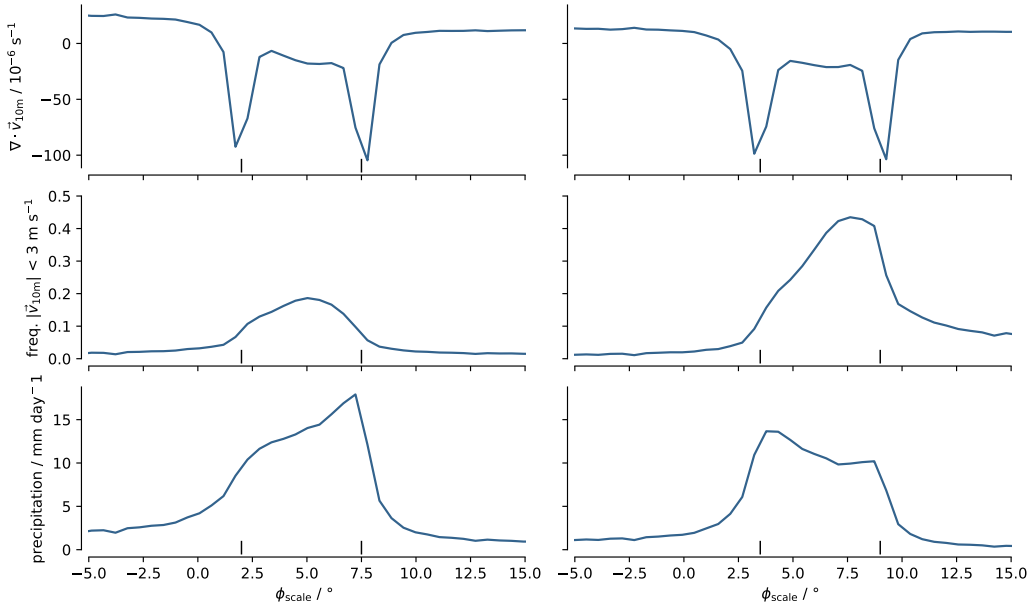

Figure 3. Zonal mean of the rescaled (top row) divergence field, (middle row) frequency of low wind speed events, and (bottom row) hourly averaged precipitation rate at (left) 38°W and (right) 23°W.

Atlantic with a pronounced peak close to ϕ_{north}. This asymmetry is most pronounced during boreal summer (not shown). We tested the dependence of our results on the chosen threshold in prominence by changing it to the 80th percentile. In this case, we almost always detect at least two convergence peaks (94.7% in the western Atlantic and 96.0% in the eastern Atlantic). Figure 3 remains qualitatively the same, though the mean latitude of both the northern and the southern edge of the ITCZ shifts poleward by about 1° and the increase of the various fields at the edges becomes less steep. To summarize, Fig. 3 shows that low wind speed events occur primarily in the inner part of the ITCZ, answering the question about how the doldrums relate to the inner life of the Atlantic ITCZ.

Temporal evolution

Finally, the mean time evolution of low wind speed events, as recorded by the PIRATA buoys, is shown in Fig. 4. For all three variables considered, i.e. surface wind speed, precipitation rate and air temperature, the temporal evolution is at least qualitatively independent of the latitude and longitude of the buoys. Surface wind speeds are characterised by a slow decrease towards $3\,\mathrm{m\,s^{-1}}$, our chosen wind speed threshold, until the onset of the low wind speed event, followed by a much faster decrease to around $1.5\,\mathrm{m\,s^{-1}}$. The wind speed then remains at this level for at least the minimum duration of the low wind speed event. The corresponding time evolution of precipitation shows average or above average precipitation rates prior to the onset of the low wind speed events and an almost complete suppression afterwards. The surface air temperature, with the exception of the PIRATA buoy at 23°W and 4°N, is reduced compared to the mean surface temperature for almost the whole time interval shown in Fig. 4. Temperature values are particularly low until the onset of the low wind speed event, which marks the beginning of a recovery in surface temperature. This pattern is consistent with what might be expected from the presence of evaporatively driven cold pools. This could also explain why

the cooling scales with the intensity of the precipitation. Taken together, these results suggest that the low wind speed events in the doldrums form in the wake of precipitating convection and are thus expected to be associated with divergence rather than convergence.

5 Discussion and Conclusion

The doldrums, a region of low wind speeds and variable wind direction in the deep tropics, have been known for centuries, but until recently have largely disappeared from mention in the scientific literature. While the doldrums are commonly associated with the convergence of the trade winds in the Intertropical Convergence Zone (ITCZ), the precise relationship is unknown. Defining the doldrums as the region of frequent low wind speed events, we show that on the timescale of multiple days the doldrums do in fact occur within the region of mean convergence that marks the ITCZ. The actual frequency of low wind events within the ITCZ is shown to depend on season and region.

Analysis of the relationship between low wind speed events and convergence on hourly time scales shows that low wind speed events peak inside the ITCZ, i.e., inside the region bounded by enhanced convergence and characterized by increased precipitation. However, the composite evolution of low wind speed events shows that the onset of low wind speeds is actually marked by a sudden absence of precipitation as well as reduced surface air temperatures. Thus low wind speed events typically occur in breaks between precipitation events in an an otherwise high-precipitation region. While this may sound counterintuitive, it is important to remember that even in the moist tropics, updrafts and precipitation occupy only a small fraction of the area at any given time. Indeed, S. T. Coleridge appeared to be aware of this lack of precipitation, the poem with which this paper began continues: "Day after day, day after day, / We stuck, nor breath nor motion; / As idle as a painted ship / Upon a painted ocean. // Water, water, every where, / And all the boards did shrink; / Water, water, every where, / Nor any drop to drink.".

Based on the result that the low wind speed events occur between the edges of the ITCZ in breaks between precipitation events, we hypothesize that the low wind speed events in the doldrums are not related to surface convergence and ascending air masses, but rather to surface divergence and descending air masses. Low wind speeds would then result from low-level surface divergence opposing the low-level inflow from the trade winds. Surface divergence could result from several processes, in particular it could be driven by gravity wave induced subsidence (Bretherton & Smolarkiewicz, 1989) or by surface density currents (e.g., Benjamin, 1968). Atmospheric surface density currents can, for example, be precipitation-driven through evaporation or condensate loading (e.g., Byers & Braham, 1949) or radiation-driven (Coppin & Bony, 2015). Testing this hypothesis requires an analysis of the relationship between low wind speed events and vertical velocity profiles to first verify whether low wind speed events are indeed related to subsidence and surface divergence, and if so, to determine what causes this surface divergence. Since the vertical structure of vertical motions in reanalyses can be highly biased (e.g., Huaman et al., 2022), this investigation is beyond the scope of the present study. One possibility to investigate this hypothesis will be to use cloud-resolving simulations in realistic setups, another might be to use idealized simulations. In the case of self-aggregation, for example, we have shown that the self-aggregation cluster, i.e., the region of increased mean precipitation bounded by intense convergence, is characterized by reduced surface wind speeds within (Windmiller & Hohenegger, 2019). In parallel to investigating this question using atmospheric models, we are also planning to investigate the low wind speed events in the doldrums using observational data collected specifically for this purpose. The relationship between low wind speed events and the area-averaged mesoscale circulation properties of vertical velocity and divergence (Bony & Stevens, 2019; George et al., 2021) within the ITCZ will be analyzed with the data collected during the upcom-

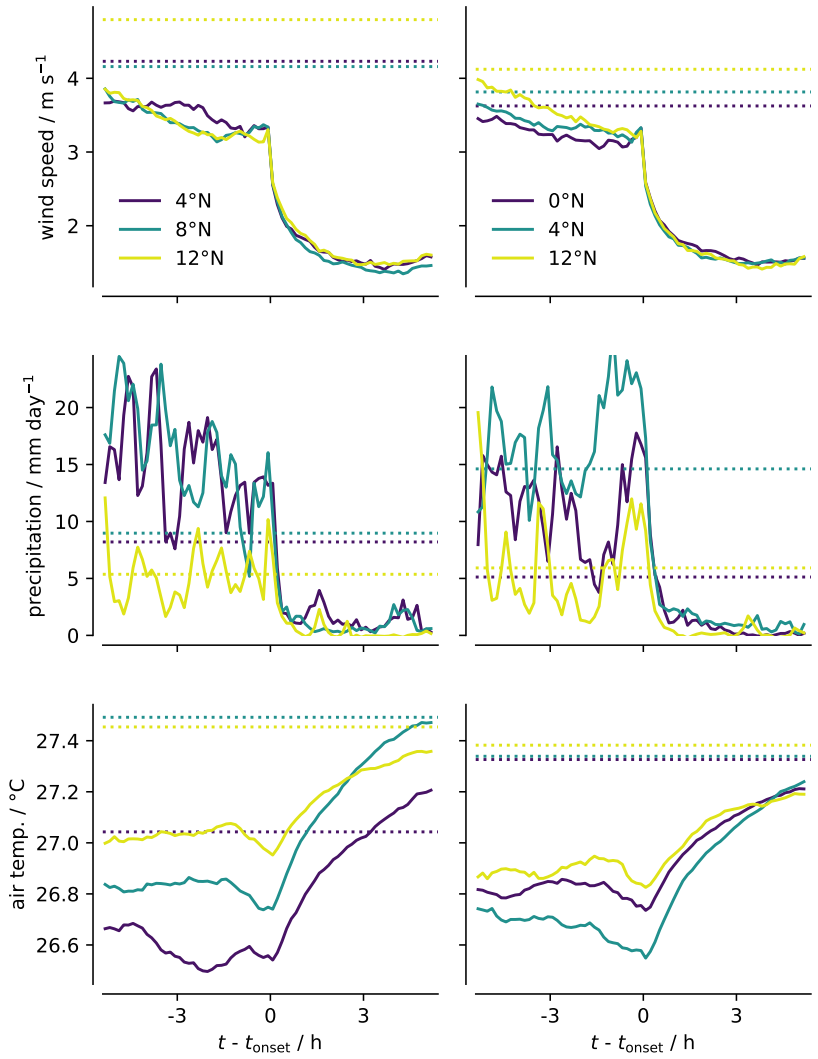

Figure 4. Time evolution of (top) surface wind speed, (middle) precipitation rate, and (bottom) surface air temperature as observed by the PIRATA buoys at (left) 38°W and (right) 23°W. The latitude of the buoy is indicated by the color. The time evolution is composited with respect to the onset time of the detected low wind speed events. The dotted lines show the monthly mean values during the month with the most frequent low wind speed events.

ing ORCESTRA campaign planned for August and September 2024 in the tropical Atlantic.

6 Open Research

All data used in this study is publicly available. NOAA Geostationary Operational Environmental Satellites (GOES) 16, 17 & 18 was accessed on 2024-02-17 from `https://registry.opendata.aws/noaa-goes`. Special Sensor Microwave Imager Sounder data (Wentz et al., 2012) was downloaded using NASA's Earth Observing System Data and Information System (EOSDIS). The data from the Pilot Research Moored Array in the tropical Atlantic (Bourlès et al., 2008) was downloaded from `https://www.pmel.noaa.gov/tao/drupal/disdel/`. The ERA5 data (Hersbach et al., 2018) was downloaded from the Copernicus Climate Change Service (C3S) Climate Data Store. The results contain modified Copernicus Climate Change Service information 2021. Neither the European Commission nor ECMWF is responsible for any use that may be made of the Copernicus information or data it contains.

Acknowledgments

The author thanks Geet George, Martin Singh, and Bjorn Stevens for helpful discussions. The author would like to further thank Martin Singh for suggesting and sending a printed copy of "The Rime of the Ancient Mariner" by S. T. Coleridge.

References

Benjamin, T. B. (1968, January). Gravity currents and related phenomena. *Journal of Fluid Mechanics*, *31*, 209–248. doi: 10.1017/S0022112068000133

Bony, S., & Stevens, B. (2019, March). Measuring Area-Averaged Vertical Motions with Dropsondes. *Journal of the Atmospheric Sciences*, *76*(3), 767–783. Retrieved 2024-03-13, from `https://journals.ametsoc.org/doi/10.1175/JAS-D-18-0141.1` doi: 10.1175/JAS-D-18-0141.1

Bourlès, B., Lumpkin, R., McPhaden, M. J., Hernandez, F., Nobre, P., Campos, E., ... Trotte, J. (2008, August). THE PIRATA PROGRAM: History, Accomplishments, and Future Directions. *Bulletin of the American Meteorological Society*, *89*(8), 1111–1126. Retrieved 2024-03-01, from `https://journals.ametsoc.org/doi/10.1175/2008BAMS2462.1` doi: 10.1175/2008BAMS2462.1

Bretherton, C. S., & Smolarkiewicz, P. K. (1989, March). Gravity Waves, Compensating Subsidence and Detrainment around Cumulus Clouds. *Journal of the Atmospheric Sciences*, *46*, 740–759. Retrieved 2013-06-20, from `http://journals.ametsoc.org/doi/abs/10.1175/1520-0469(1989)046<0740:GWCSAD>2.0.CO;2` doi: 10.1175/1520-0469(1989)046⟨0740:GWCSAD⟩2.0.CO;2

Byers, H. R., & Braham, R. R. (1949). *The Thunderstorm: Report of the Thunderstorm Project (a joint project of four U.S. Government Agencies : Air Force, Navy, National Advisory Committee for Aeronautics, and Weather Bureau)* (Tech. Rep.). Washington, D.C.. doi: 10.1002/qj.49707733225

Coppin, D., & Bony, S. (2015, December). Physical mechanisms controlling the initiation of convective self-aggregation in a General Circulation Model. *Journal of Advances in Modeling Earth Systems*, *7*, 2060–2078. (ISBN: 0140917101) doi: 10.1002/2015MS000571

Cox, C., & Munk, W. (1954, November). Measurement of the Roughness of the Sea Surface from Photographs of the Sun's Glitter. *Journal of the Optical Society of America*, *44*(11), 838. Retrieved 2024-03-20, from `https://opg.optica`

.org/abstract.cfm?URI=josa-44-11-838 doi: 10.1364/JOSA.44.000838

Durst, C. S. (1926). The doldrums of the Atlantic. *Geophysical Memoirs*, *28*, 229–237.

Fletcher, R. D. (1945, September). THE GENERAL CIRCULATION OF THE TROPICAL AND EQUATORIAL ATMOSPHERE. *Journal of Meteorology*, *2*, 167–174. doi: 10.1175/1520-0469(1945)002⟨0167:TGCOTT⟩2.0.CO;2

Gentilli, J. (2005). Doldrums. In J. E. Oliver (Ed.), *Encyclopedia of World Climatology* (pp. 338–338). Springer Netherlands. Retrieved 2024-03-06, from http://link.springer.com/10.1007/1-4020-3266-8_69 (Series Title: Encyclopedia of Earth Sciences Series) doi: 10.1007/1-4020-3266-8_69

George, G., Stevens, B., Bony, S., Pincus, R., Fairall, C., Schulz, H., ... Radtke, J. (2021, November). JOANNE: Joint dropsonde Observations of the Atmosphere in tropical North atlaNtic meso-scale Environments. *Earth System Science Data*, *13*(11), 5253–5272. Retrieved 2023-11-09, from https://essd.copernicus.org/articles/13/5253/2021/ doi: 10.5194/essd-13-5253-2021

Gordon, A. H. (1951, April). Seasonal variation of the axes of low-latitude pressure and divergence patterns over the oceans. *Quarterly Journal of the Royal Meteorological Society*, *77*(332), 302–306. Retrieved 2024-03-06, from https://rmets.onlinelibrary.wiley.com/doi/10.1002/qj.49707733215 doi: 10.1002/qj.49707733215

Herrmann, B., & Wolfers, A. (2021). *Allein zwischen Himmel und Meer: meine achtzig Tage beim härtesten Segelrennen der Welt.* München: C. Bertelsmann.

Hersbach, H., Bell, B., Berrisford, P., Biavati, G., Horányi, A., Muñoz Sabater, J., ... Thépaut, J.-N. (2018). *ERA5 hourly data on single levels from 1959 to present. Copernicus Climate Change Service (C3S) Climate Data Store (CDS) (Accessed on 21-11-2021), 10.24381/cds.adbb2d47.*

Huaman, L., Schumacher, C., & Sobel, A. H. (2022). *Assessing the Vertical Velocity of the East Pacific ITCZ.* (Pages: e2021GL096192 Publication Title: Geophysical Research Letters Volume: 49) doi: 10.1029/2021GL096192

Klocke, D., Brueck, M., Hohenegger, C., & Stevens, B. (2017, December). Rediscovery of the doldrums in storm-resolving simulations over the tropical Atlantic. *Nature Geoscience*, *10*(12), 891–896. Retrieved 2017-11-22, from http://www.nature.com/articles/s41561-017-0005-4 doi: 10.1038/s41561-017-0005-4

Köhler, L., Windmiller, J. M., Baranowski, D., Brennek, M., Ciuryło, M., Hayo, L., ... Tuinder, O. (2024). *Calm ocean, stormy sea: Atmospheric and oceanographic observations of the Atlantic during the ARC ship campaign* [Paper submitted for publication to ESSD].

Mapes, B. E., Chung, E. S., Hannah, W. M., Masunaga, H., Wimmers, A. J., & Velden, C. S. (2018, January). The Meandering Margin of the Meteorological Moist Tropics. *Geophysical Research Letters*, *45*, 1177–1184. (Publisher: John Wiley & Sons, Ltd) doi: 10.1002/2017GL076440

Masunaga, H. (2023, May). The Edge Intensification of Eastern Pacific ITCZ Convection. *Journal of Climate*, *36*(10), 3469–3480. Retrieved 2023-06-09, from https://journals.ametsoc.org/view/journals/clim/36/10/JCLI-D-22-0382.1.xml doi: 10.1175/JCLI-D-22-0382.1

Masunaga, H., & Mapes, B. E. (2020, February). A Mechanism for the Maintenance of Sharp Tropical Margins. *Journal of the Atmospheric Sciences*, JAS–D–19–0154.1. Retrieved 2020-02-28, from http://journals.ametsoc.org/doi/10.1175/JAS-D-19-0154.1 doi: 10.1175/jas-d-19-0154.1

Maury, M. F. (1855). *The physical geography of the sea.* London: Sampson, Low, Son & Co. Retrieved 2024-03-05, from https://www.biodiversitylibrary.org/bibliography/102148 doi: 10.5962/bhl.title.102148

May, R., Arms, S., Marsh, P., Bruning, E., Leeman, J., Bruick, Z., & Camron, M. D.

(2016). *MetPy: A Python Package for Meteorological Data.* [object Object]. Retrieved 2024-03-04, from https://www.unidata.ucar.edu/software/metpy/ (Language: en) doi: 10.5065/D6WW7G29

Riehl, H., & Malkus, J. S. (1958). On the Heat Balance in the Equatorial Trough Zone. *Geophysica*, *6*(2), 503–538.

Virtanen, P., Gommers, R., Oliphant, T. E., Haberland, M., Reddy, T., Cournapeau, D., ... Vázquez-Baeza, Y. (2020, March). SciPy 1.0: fundamental algorithms for scientific computing in Python. *Nature Methods*, *17*(3), 261–272. Retrieved 2023-08-14, from https://www.nature.com/articles/s41592-019-0686-2 doi: 10.1038/s41592-019-0686-2

Weller, E., Shelton, K., Reeder, M. J., & Jakob, C. (2017, May). Precipitation associated with convergence lines. *Journal of Climate*, *30*, 3169–3183. (Publisher: American Meteorological Society) doi: 10.1175/JCLI-D-16-0535.1

Wentz, F., Hilburn, K., & Smith, D. (2012). *RSS SSMIS Ocean Product Grids Daily from DMSP F17 netCDF.* [object Object]. Retrieved 2024-03-20, from https://cmr.earthdata.nasa.gov/search/concepts/C1996546695-GHRC_DAAC.html doi: 10.5067/MEASURES/DMSP-F17/SSMIS/DATA301

Windmiller, J. M., & Hohenegger, C. (2019, December). Convection On the Edge. *Journal of Advances in Modeling Earth Systems*, *11*(12), 3959–3972. Retrieved 2020-02-21, from https://onlinelibrary.wiley.com/doi/abs/10.1029/2019MS001820 (Publisher: John Wiley & Sons, Ltd) doi: 10.1029/2019MS001820

Windmiller, J. M., & Stevens, B. (2024, January). The inner life of the Atlantic Intertropical Convergence Zone. *Quarterly Journal of the Royal Meteorological Society*, *150*(758), 523–543. Retrieved 2024-02-19, from https://rmets.onlinelibrary.wiley.com/doi/10.1002/qj.4610 doi: 10.1002/qj.4610

Wodzicki, K. R., & Rapp, A. D. (2016). Long-term characterization of the Pacific ITCZ using TRMM, GPCP, and ERA-Interim. *Journal of Geophysical Research: Atmospheres*, *121*, 3153–3170. doi: 10.1002/2015JD024458

Yanai, M., Esbensen, S., & Chu, J. (1973). Determination of bulk properties of tropical cloud clusters from large-scale heat and moisture budgets. *Journal of the Atmospheric Sciences*, *30*(4), 611–627.

Figure 2.

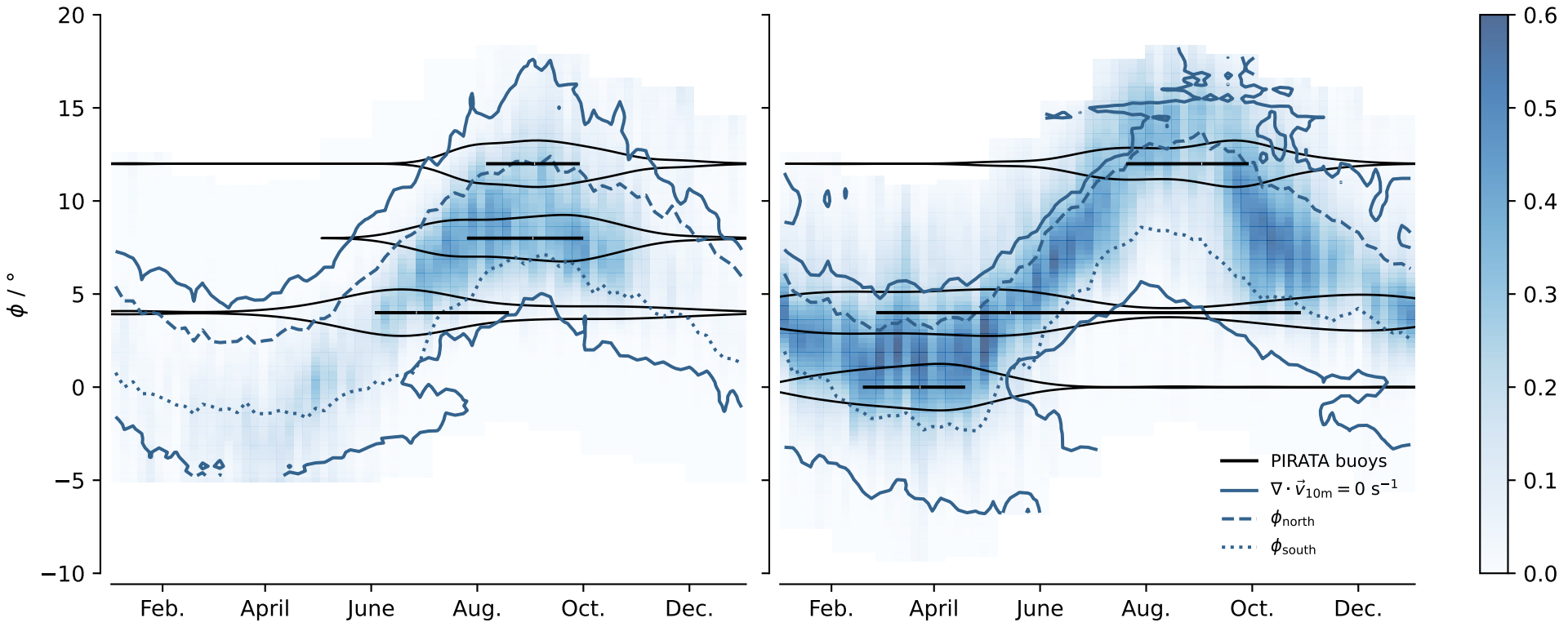
20
15
10
5
0
−5
−10
ϕ / °
Feb.
April
June
Aug.
Oct.
Dec.
Feb.
April
June
Aug.
Oct.
Dec.
PIRATA buoys
$\nabla \cdot \vec{v}_{10m} = 0\ s^{-1}$
ϕ_{north}
ϕ_{south}
0.6
0.5
0.4
0.3
0.2
0.1
0.0

Figure 3.

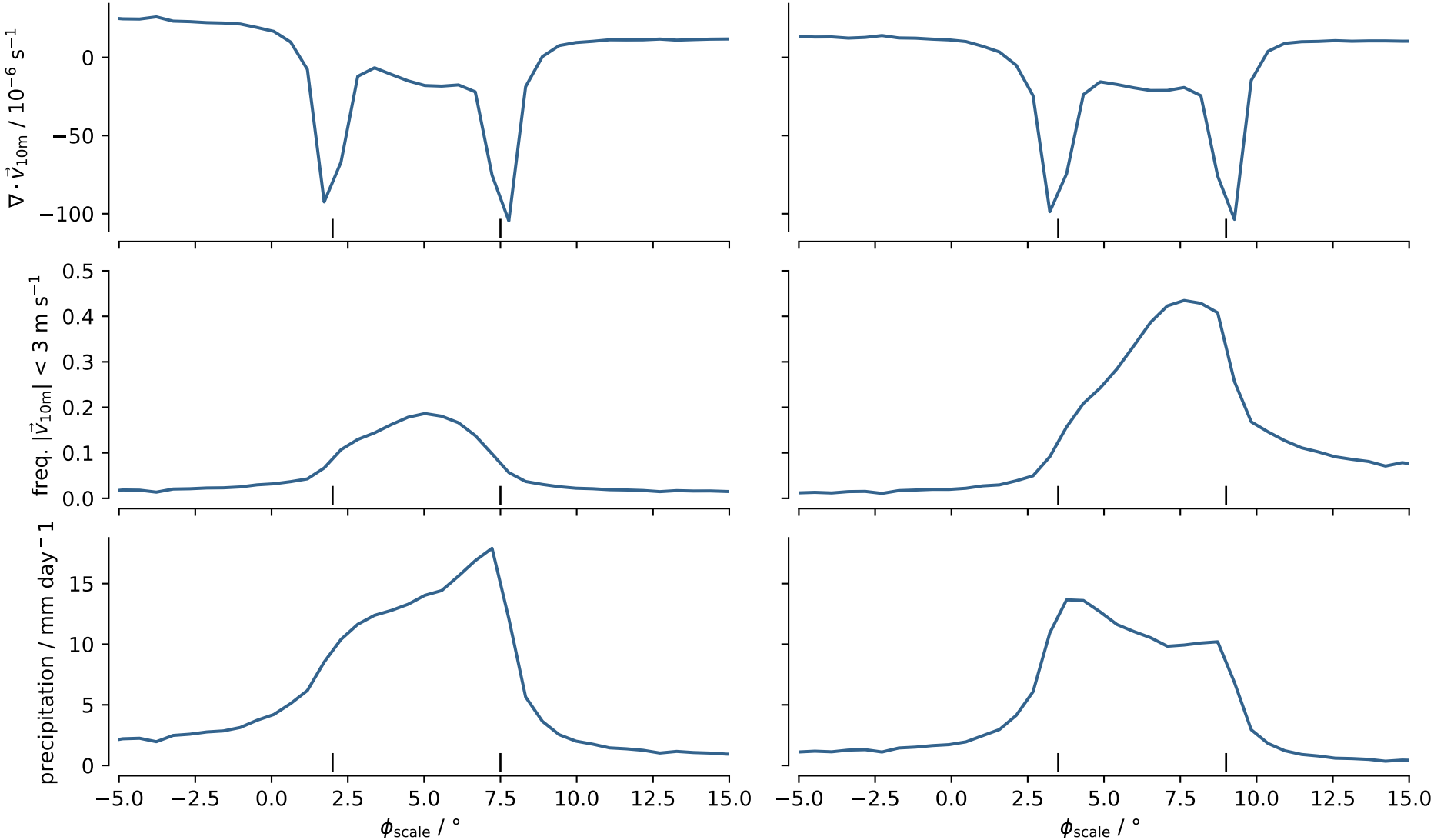
$\nabla \cdot \vec{v}_{10m}$ / 10^{-6} s^{-1}
0
−50
−100
freq. $|\vec{v}_{10m}| < 3$ m s^{-1}
0.5
0.4
0.3
0.2
0.1
0.0
precipitation / mm day^{-1}
15
10
5
0
−5.0
−2.5
0.0
2.5
5.0
7.5
10.0
12.5
15.0
ϕ_{scale} / °

Figure 4.

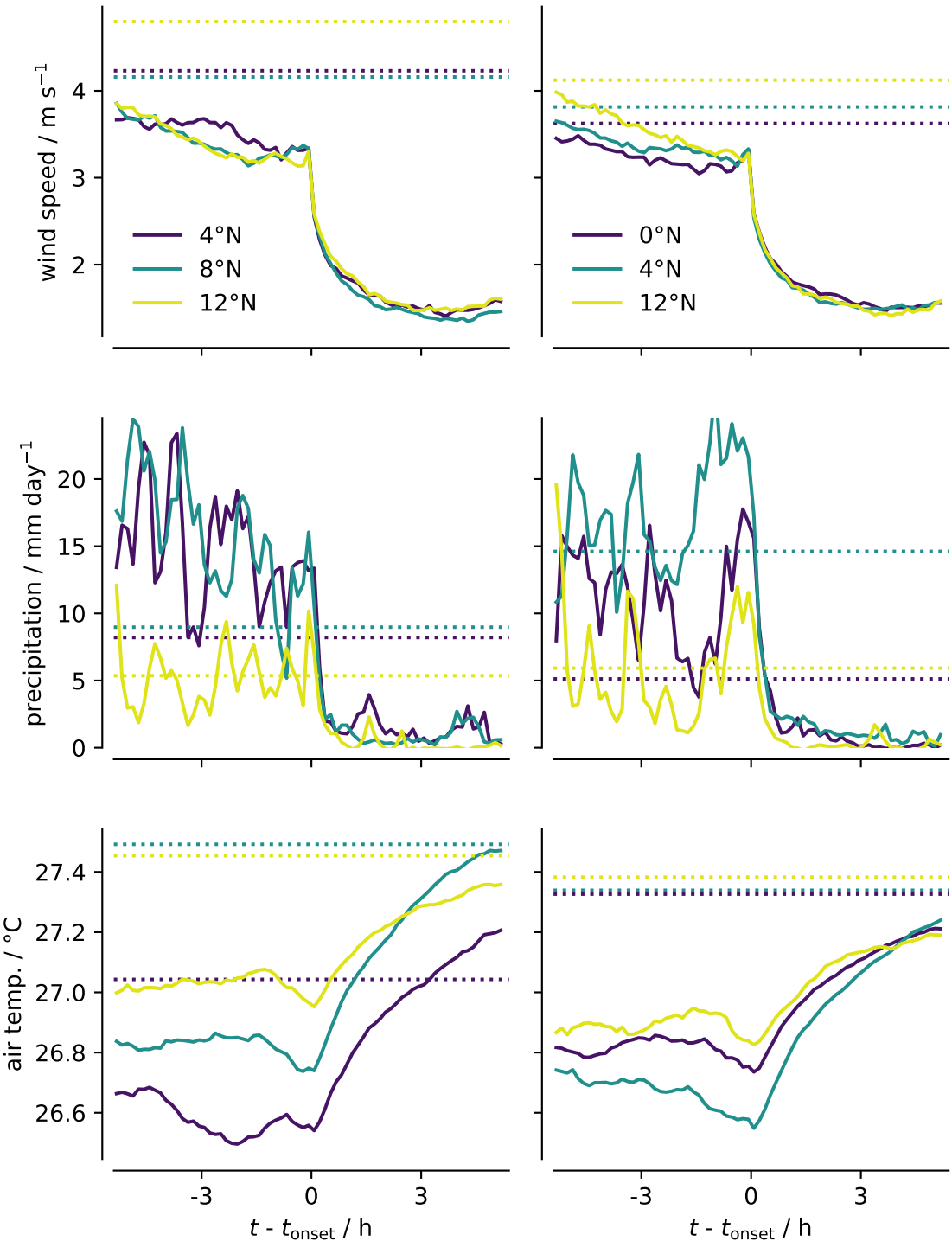
wind speed / m s^{-1}
4
3
2
4°N
8°N
12°N
0°N
4°N
12°N
precipitation / mm day^{-1}
20
15
10
5
0
air temp. / °C
27.4
27.2
27.0
26.8
26.6
-3
0
3
t - t_{onset} / h
-3
0
3
t - t_{onset} / h

Figure 1.